Strain-Induced Spectral Red-Shifting from Nanoscale Frustum Arrays Fabricated over InGaN/GaN Quantum Wells for Light-Emitting Applications

Wai Yuen Fu and Hoi Wai Choi*

Department of Electrical and Electronic Engineering, the University of Hong Kong, Pokfulam Road, Hong Kong

E-mail: hwchoi@hku.hk

Abstract

While spectral blue-shifting caused by nano-structuring of InGaN/GaN quantum wells has been widely reported for altering the emission color of light-emitting diodes, the same cannot be said for spectral red-shifting. It is well known that nano-structuring of the quantum wells gives rise to relaxation of the strain incurred in the quantum wells, reducing the Quantum Confined Stark Effect with a consequence of spectral shifting to shorter wavelengths. In this report, we demonstrate a nanostructure configuration that produces the opposite effect- spectral red-shifting- by increasing the strain in the quantum wells through the formation of an inverted nano-conical-frustum array over the quantum wells, without allowing the nanostructures to penetrate through the quantum wells. Under such conditions, spectral red-shifting of the photoluminescence spectrum can be observed, consistent with the prediction of strain induction in the quantum wells by molecular dynamics simulations. Experimentally, spectral red-shift of the

photoluminescence spectrum by up to 7.6 nm has been observed, when the proposed nanostructures are fabricated on InGaN/GaN quantum wells grown on *c*-plane sapphire substrate with nominal emission wavelength of ~560 nm.

Keywords

Strain engineering, bandgap engineering, gallium nitride, nanosphere lithography, molecular dynamics, UV Raman

1 Introduction

Solid-state lighting based on III-Nitride light-emitting diodes (LEDs) are becoming the dominant forms of electrical lighting throughout the worldwide owing to their energy efficiencies compared to incandescent and gas discharge sources.[1] Currently, commercially available white-light LEDs rely on color down-converters such as phosphors or quantum dots[2,3] to generate the desired broadband spectrum. However, such color conversion processes inevitably give rise to a loss of efficiency due to the Stokes shift, in addition to reduced lifetimes and reliabilities. To avoid such efficiency losses which is important for applications such as lighting and color displays, multiple LEDs, typically of the primary colors red, green and blue (RGB), can be used simultaneously to generate the various different required colors to avoid color conversion. However, the green III-nitride LEDs are generally less efficient that their blue counterparts, while phosphide-based red LEDs are routinely used, a consequence based on a phenomenon known as the "green gap". Apart from the drastic reductions of internal quantum efficiencies (IQE) of InGaN/GaN quantum wells with increasing In content,[4] the amount of Indium (In) that could be incorporated is also limited due to the low miscibility of Indium in GaN.[5] This has been and remains one of the key challenges in III-nitride technology.

While the growth of high Indium content quantum wells represents a great challenge,

strain engineering may well be a good complementary approach towards achieving longer wavelength emission with the highly-strained InGaN/GaN quantum wells, with nano-structuring being one common means of achieving such goals.[6] In fact, the incorporation of nanostructures has extensively been employed for altering the emission color of LEDs[7–12] through spectral shifting, although only spectral shifting towards shorter wavelengths (blue-shifting) has been reported. For the group III-nitrides, the In content in the quantum wells not only determines the color of emission, but also the extents of strains. The strain in the quantum wells give rise to the Quantum Confined Stark Effect (QCSE) which reduces IQEs and make emission wavelengths sensitive to current injection levels. Nano-structuring of the quantum wells has been demonstrated to alleviate the effects of QCSE in many reports via the strain relaxation effect.[8,11,13] One application is the demonstration of a monolithic broadband LED based on graded strain relaxation of the InGaN/GaN quantum wells through non-uniform nano-structuring.[14]

Nevertheless, strain relaxation via nano-structuring can only lead to spectral blue-shifting, while the ability to spectral red-shift will find invaluable applications in longer wavelength emitting InGaN LEDs, including the possibilities of red InGaN LEDs. As such, we attempt to modify the nanostructure configuration so that an increase of strain in the quantum wells can be achieved, as opposed to relaxing the strain, adopting a top-down fabrication approach. According to our previous studies on the strain relaxation mechanism of micropillars and its relation to emission color,[15] a relative spectral red-shift at the edges of microdisks with low Indium content quantum wells compared to the centers of the microdisks has been observed through scanning near-field optical spectroscopy (SNOS), attributed to a local increase in strain field. Such unexpected observations inspire the design of the currently proposed structures.

In this study, we report on the design, fabrication and characterization of an inverted nano-conical-frustum array that is capable of inducing spectral red-shifts in InGaN/GaN quantum wells via strain induction for light-emitting applications. Molecular dynamics sim-

ulations and $\mathbf{k} \cdot \mathbf{p}$ calculations are employed to design and analyze the nanostructure, while photoluminescence (PL) and Raman studies are carried out on the fabricated nanostructures to verify the validity and feasibility of the proposed approach.

2 Design and Simulation

In typical nano-structuring schemes of InGaN/GaN quantum wells that are intended for spectral blue-shifting, the nanostructures are fabricated by etching through the quantum wells. The exposed sidewalls allow the strained quantum well layers to relax, reducing the QCSE and thus inducing a spectral blue-shift. Therefore, to design a nanostructure that induces spectral shifting in the opposite direction, the quantum wells must be left intact.

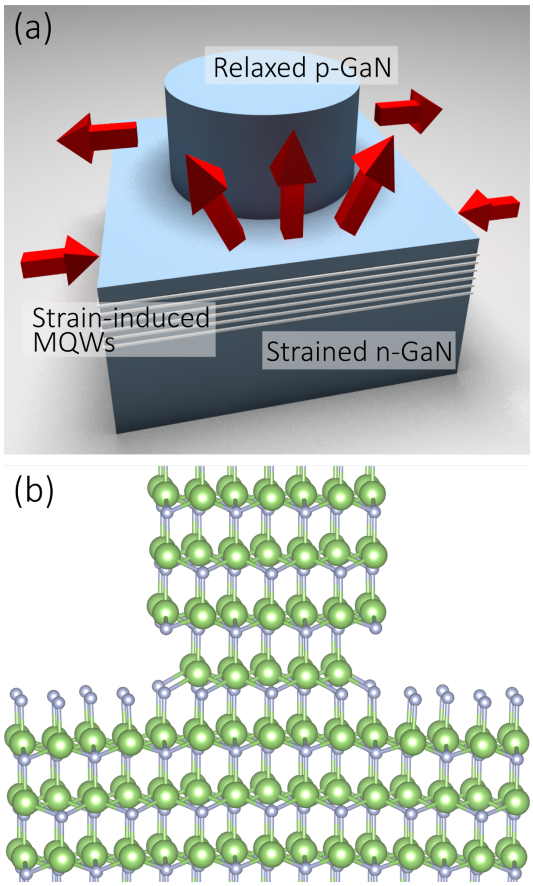

Figure 1: (a) Schematic diagram of the strain induction mechanism invoked by fabricating a nanostructure above the MQWs; and (b) the schematic atomic arrangement of a nanostructure inducing strain to the region underneath it.

One viable option is formation of the nanostructures over the quantum wells, which would invoke a series of complicated but intertwining strain mechanisms. Relaxation of in-plane strain, originating from thermal mismatch amongst the various epitaxially grown layers at different temperatures as well as the sapphire substrate, will occur in the nanostructures as the atoms are displaced outwards towards the sidewalls. As the crystal lattice underneath the nanostructures are still experiencing in-plane strain caused by lattice and thermal mismatches, the atoms at the bases of the nanostructures tend to be pulled upwards and outwards due to the nature of the strong ionic-covalent bonds of wurtzite III-nitrides, thus increasing the tensile out-of-plane strain. Consequentially, if the quantum wells are positioned at the bases of the nanostructures, the increase in the out-of-plane strain will lead to spectral red-shifting due to an increase in the QCSE, similar to the red-shifting effect incurred by an increase in local out-of-plane strain at the edges of the micropillars in a previous study.[15] A schematic diagram of the proposed strain-inducing nanostructure is illustrated in Fig. 1(a), with the directions of atomic movements as indicated by the red arrows, while Fig. 1(b) shows the schematic atomic arrangement near the nanostructure/film interface highlighting the atomic shifts. By maximizing strain relaxation of the nanostructure and its proximity to the quantum wells, as well as minimizing its interfacial area, the extent of spectral red-shift can be maximized. The obvious geometry derived from such optimization rules would be that of an inverted nano-conical frustum. A 2D molecular dynamics study is undertaken to compare the effects of strain induction between such inverted nano-conical frustum with typical non-tapered nanopillars of base diameters ranging from 10 nm to 100 nm, set up using c-plane wurtzite GaN blocks. The simulations are carried out using the software package LAMMPS[16] with a Stillinger-Weber potential[17] for InAlGaN[18–20] on a structure corresponding to the wafer used in the experiments. The GaN blocks are fixed at the bottom ($y = 0$) with a compressive strain of 0.023% to emulate a boundary that is lattice-matched to a partially relaxed GaN buffer with a biaxial stress of 1 GPa. For simplicity, only a single quantum well of 4.7 nm thickness is implemented and positioned directly underneath the

nanostructure.

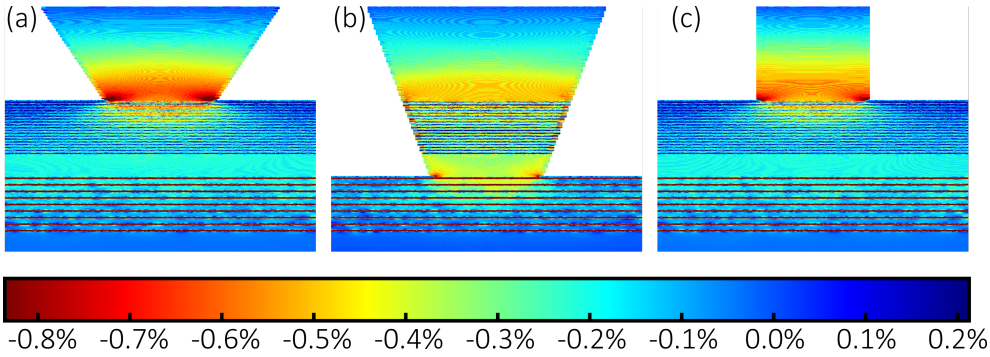

Figure 2: Molecular dynamics simulations of the out-of-plane strain of an inverted nano-conical frustum (a) over the EBL layer, (b) over the MQWs; and (c) a nanopillar over the EBL layer; all with 50 nm base diameters. The color bar for the strain fields is on the far right, with the negative value representing tensile out-of-plane strain, and vice versa.

As shown in Fig. 2, the out-of-plane strain field of the nanostructures are extracted from the molecular dynamic simulations. With the diameter at the top of the nanostructure kept constant, as the interfacial area between the nano-frustum and the underneath region is reduced, the strain field becomes increasingly concentrated, the out-of-plane strain increases from -2.1% to -2.6% when the base diameter decreases from 100 nm to 10 nm. On the other hand, part of the neighboring etched and exposed region becomes strained-relaxed. The extracted strain field is then used in $\mathbf{k} \cdot \mathbf{p}$ calculations to estimate the spectral shift as plotted in Fig. 3. The $\mathbf{k} \cdot \mathbf{p}$ perturbation theory is used to solve the Schrödinger equation following the steps described in Ref. 21–23. As can be seen, the largest extent of spectral red-shift, averaged across all 9 pairs of quantum wells, of around 10 nm is induced when the base diameter of the inverted nano-conical frustum is 100 nm, with a top diameter of about 150 nm, positioned above the AlGaN/GaN EBL. It seems that the etching of the tensile-strained EBL limits the strain induced in the quantum wells. As for non-tapered nanopillars, the extent of red-shift decreases once the bottom diameter reaches 50 nm. According to Fig. 3, the largest extent of spectral red-shift can be achieved by tapering the nanopillars with diameter of around 100 nm to 150 nm to form inverted nano-conical frustum.

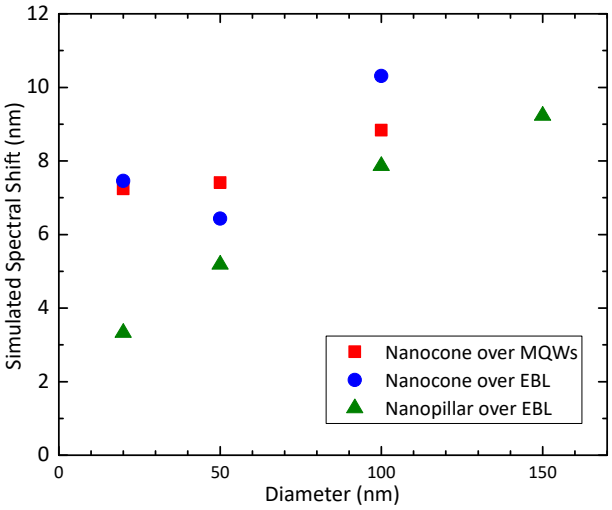

Figure 3: Simulated average spectral red-shifts of the strain-inducing nanostructures.

3 Results and discussion

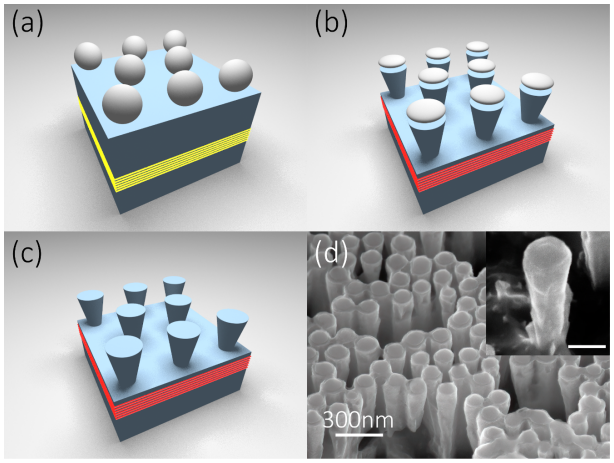

Figure 4: The inverted nano-conical frustums are fabricated by first (a) undertaking the nanosphere lithography, followed by subsequent (b) ICP etch under high pressure; (c) thus resulting in inverted nano-conical frustums; (d) an SEM image of an array of InGaN/GaN inverted nano-conical frustums with 9° inclination angle and around 150 nm-diameter, with an inset showing a zoomed in SEM image of an individual inverted nano-conical frustums. Scale bar in the inset is 100 nm.

The nanostructures are fabricated using a top-down approach on a metal-organic vapour-phase epitaxy (MOVPE) grown wafer on a *c*-plane patterned sapphire substrate. There is a 5 μm -thick undoped-GaN buffer layer, on top of which is a 1.7 μm -thick n-GaN layer. The MQWs, containing 9 pairs of InGaN/GaN quantum wells, are grown on the n-

GaN layer. Above the MQWs is a 70 nm-thick p-GaN spacer, followed by an AlGaN/GaN electron blocking layer (EBL). The structure is then capped with a 330 nm-thick p-GaN layer. The average Indium composition of about 20% in the quantum wells is estimated using TEM energy dispersive x-ray spectroscopy (EDX), while the nominal emission wavelength is ~560 nm. The fabrication process flow is illustrated in Fig. 4(a) to (c). For rapid prototyping, nanosphere lithography has been utilized similar to our previous studies.[24–27] Firstly, silica nanospheres with an average diameter of 150 nm are spin-coated onto the surface of the entire wafer, as depicted in Fig. 4(a). Subsequently, ICP etching is undertaken with the nanospheres as masks to form round-shaped nanostructures, as shown in Fig. 4(b). For reverse-tapering, the ICP etch is conducted at a higher pressure of 55 mTorr.[28] Fig. 4(c) illustrates the inverted nano-conical frustums that are formed after removal of the residual nanospheres, while 45-degree-tilted SEM images of the fabricated inverted nano-conical frustums are shown in Fig. 4(d).

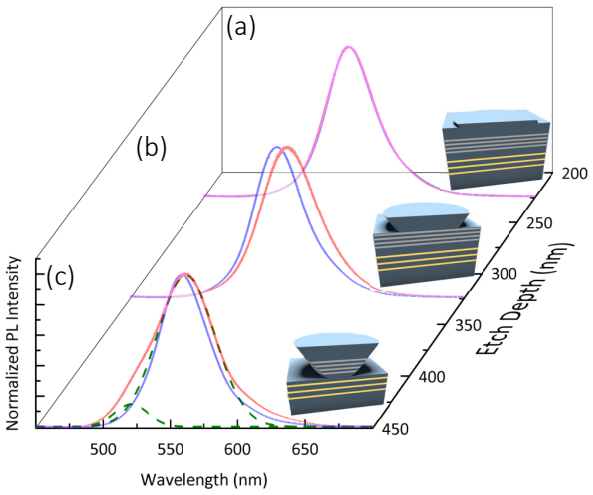

Figure 5: PL spectra of MQWs' emission with inverted nano-conical frustum array etched (a) to 225 nm depth in the p-GaN layer; (b) 325 nm depth and close to the MQWs; and (c) 450 nm depth, where the etch terminates right above the MQWs. The blue curves are the corresponding PL spectra of the as-grown for reference purpose. The green dashed lines in (c) represent the Gaussian fitted curves for spectral-shifts in both blue and red directions.

Room-temperature micro-photoluminescence (μ-PL) spectra of the strain-inducing inverted nano-conical frustum array are conducted. A Coherent CUBE 405 nm continuous-

wave (CW) diode laser source, operated at 3 mW, is used to excite PL emission from the samples. The PL signal is coupled to and dispersed by a 600 l/mm grating in a Horiba iHR550 spectrometer and detected by a Syncerity back-illuminated charged coupled device (CCD). The PL spectra of the inverted nano-conical frustum array with etch depths of 225 nm, 325 nm and 450 nm are plotted in Fig 5. To verify that the trends of spectral red-shifts is not merely an artefact arising from sample-to-sample variations, the experiments have been repeated 3 times using different samples from the same wafer. The dependence of the average spectral red-shift from the 3 sets of data with respect to the etch depth is summarized in Fig. 6. Note that a small dependence of the reverse-tapering angle with the etch depth is observed. The magnitudes of spectral red-shift are averaged over all 3 runs with the variation between runs indicated by the error bars.

Starting from top surface, there is only a mild spectral red-shift of 0.2 nm and an increase in spectral width by 1.5 nm when the etch depth is ~225 nm, i.e., etched to the middle of the p-GaN layer, as shown in Fig. 5(a), in which the spectra of as-grown and the etched sample largely overlap with each other. For consistency, all spectral widths mentioned this manuscript refer to their full-widths-at half maximum (FWHM). When the etch depth extends to ~325 nm, i.e., close to but not etched through the AlGaN/GaN EBL, the maximum spectral red-shift of 7.6 nm can be observed from the PL spectrum in Fig. 5(b), consistent with predictions by the aforementioned simulations as shown in Fig. 3. Broadening of the spectra by 5.9 nm is also observed, as the shorter wavelength side of the emission peak appears to have a lesser extent of spectral red-shift than that of the longer wavelength side. This is attributed to the strain gradient induced by the nanostructure, as evident from the strain field map shown in Fig. 2(a). The closer the quantum well layer is to the nanostructure, the more induced strain it can experience. Specially, for an inverted nano-conical frustum with a base diameter of 100 nm situated on top of the EBL, the out-of-plane strain of the top-most quantum well to the bottom quantum well varies from -2.1% to -1.9%, as estimated from the molecular dynamic simulations. The strain gradient thus causes each quantum well layer

underneath the nanostructure to exhibit different extents of spectral red-shifts, leading to spectral broadening. Nevertheless, due to the larger separation between the MQWs and the nanostructure in the presence of the EBL, the induced strain field exerted by the inverted nano-conical frustum can be applied uniformly in the horizontal direction, covering regions even not right underneath the nanostructure itself.

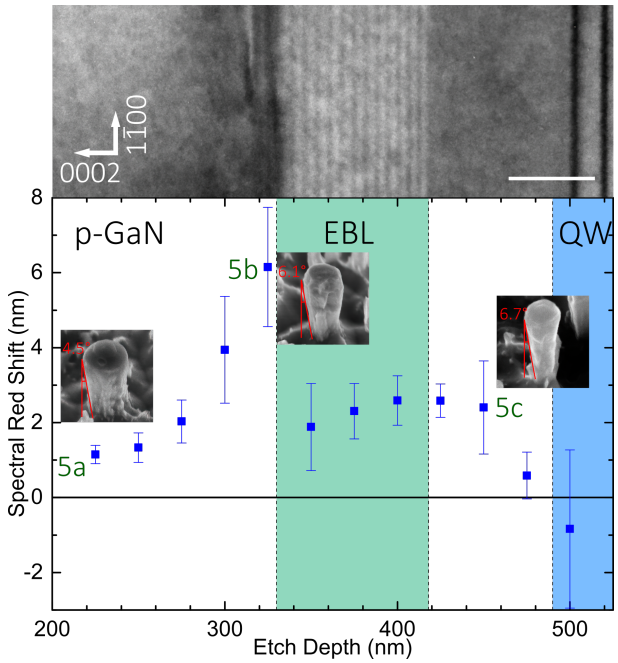

Figure 6: Calculated average spectral red-shifts from 3 samples induced by the inverted nano-conical frustums by deducing the change in PL emission peak wavelength via Gaussian fitting. Note that the reverse-tapering angle also slightly changes with the etch depth, as demonstrated by the 45-degree-tilted SEM images in the inset. Above the graph is a cross-sectional TEM image of the sample taken along the [11$\bar{2}$0] zone axis, sized to correspond to the x-axis of the graph (The scale bar is 50 nm).

At an etch depth of 450 nm, the sidewalls of the AlGaN/GaN EBL are exposed, resulting in relaxation of the tensile-strained AlGaN layers. The increase in the in-plane compressive strain of the AlGaN layer thus lead to overall strain relaxation in the other layers, including the quantum wells underneath, thus causing a spectral blue-shift. Under this circumstance, strain induction only occurs at the upper 5 quantum wells underneath the nanostructure, as the strain induced in the lower 4 quantum wells would not overcome the relaxed strain due to relaxation of the AlGaN/GaN EBL, exhibiting a decrease in the average out-of-plane

strain from around -2.2% for the upper 5 quantum wells to around -1.9% for the lower four quantum wells, according to molecular dynamics simulations. With the superposition of the strain relaxation effect caused by relaxation of the AlGaN/GaN EBL, as well as the highly confined strain field induced by the nanostructure at close proximity to the quantum wells, the actual region that exhibit a net increase in strain is smaller, albeit to a larger degree. This is reflected in the molecular dynamics simulated strain field shown in Fig. 2(c), showing that the quantum wells are strain-relaxed and strain-induced simultaneously. This implies that both spectral blue-shift and spectral red-shift are occurring concurrently after etching, contributing to a relatively larger spectral broadening. The broadened spectrum, with an increase in width by 9.9 nm, contains two distinguishable emission peaks, corresponding to a spectral red-shift of 2.3 nm and a spectral blue-shift of 38.5 nm simultaneously, as illustrated in Fig. 5(c). This is also reflected in the sharp jump in the *average* spectral shift that changes from 6.2 nm to 1.9 nm, as shown in Fig. 6, when the etch exceeds the interface of p-GaN and the EBL. Note that the smaller change in the *average* spectral shift is due to single peak-fit of the spectra that broadens in both directions. A cross-sectional bright field TEM image, taking along the $[11\bar{2}0]$ zone axis by a FEI Tecnai G2 20 TEM, showing the sample's wafer structure at corresponding etch depth is placed on top of the graph in Fig. 6 for illustrative purpose.

Ultraviolet (UV) Raman spectroscopy is further carried out to study the changes in strain conditions in the samples due to the nanostructures. A 325 nm He-Cd laser (Kimmon, ik3301R-G) is used to excite the sample under a back scattering $z(xx)\bar{z}$ configuration. Using a UV source for excitation minimizes overlap between the Raman signal and the PL signal. Moreover, as the laser wavelength is below the absorption peak of GaN, the UV laser signal would readily be absorbed by the material, so that the Raman signals are only primarily generated from regions close to the sample surface, where the inverted nano-conical frustum array and the quantum wells are situated. This Raman signal is then analyzed by the same spectrometer using a 2400 l/mm grating.

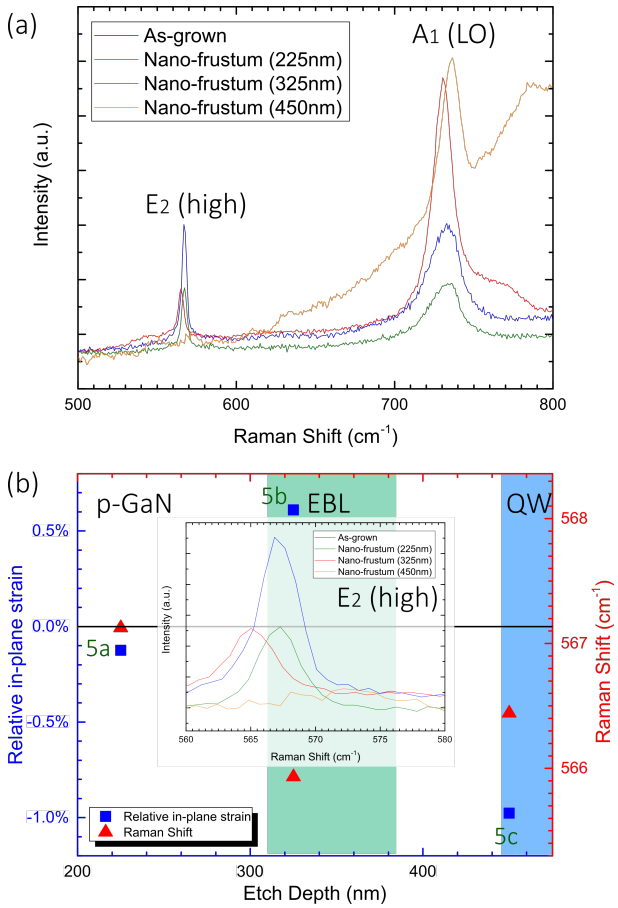

Figure 7: (a) Raman spectra of red-shift inducing nano-frustums at 3 different etch depths; (b) estimated in-plane strain (relative to the as-grown) calculated from the E_2 (high) and A_1 (LO) peak values. Inset shows the zoomed-in graphs of the E_2 (high) peak.

Fig. 7(a) shows the measured Raman spectra of the strain-inducing inverted nano-conical frustum array at different etch depth, together with the spectrum of the as-grown sample as a reference. The estimated in-plane strain relative to the as-grown sample, as calculated using the peak values of the E_2 (high) and A_1 (LO) from the Raman spectra,[29,30] are shown in Fig. 7(b). For the as-grown sample, two Raman spectral peaks are observed at 567.1 cm^{-1} and 732.1 cm^{-1}, which can be attributed to the E_2 (high) and A_1 (LO) phonon modes, respectively.[29,30] The initial etch to a depth of 225 nm barely shifts the Raman peaks, which are observed at 567.1 cm^{-1} and 731.6 cm^{-1} respectively. These correspond to a relative in-plane strain of -0.125%. The negligible change in strain is expected as the PL peaks in Fig. 5(a) also show little to no shift as well. When the etch depth reaches 325 nm, the Raman peaks shift to 566.6 cm^{-1} and 734.4 cm^{-1}, corresponding to a relative in-plane strain of 0.6%. The higher compressive strain causes the emission peak to spectral red-shift, as shown in Fig. 5(b). When the etch depth reaches 450 nm, however, the Raman peaks are now observed at 566.4 cm^{-1} and 727.8 cm^{-1}, corresponding to a relative in-plane strain of -0.9%. This means that the sample is now more strain-relaxed than the as-grown sample, thus causing the emission to blue-shift as illustrated in Fig. 5(c). The overall trend of the in-plane strain as calculated from the Raman peak values correlates well with the PL measurements as well as the molecular dynamics studies, offering solid evidence that the spectral red-shift is caused by the strain-inducing inverted nano-conical frustum array.

Time-resolved PL (TRPL) study has also been carried out to investigate the change in QCSE due to the inverted nano-conical frustum array. The TRPL measurement is performed using a PicoQuant time-correlated single photon counting system. A 405 nm picosecond pulsed laser source, PicoQuant LDH-405, controlled by a PDL-800D driver, is used to excite the sample at a repetition rate of 10 MHz. The PL signal after filtered by a dichroic mirror and longpass filter at 420 nm, are then received by an MPD PDM Single Photon Avalanche Diode (SPAD) detector. The timings of the received photons are analyzed using a Picoquant PicoHarp 300 TCSPC module. Plotted in Fig. 8 are the TRPL spectra of the strain-inducing

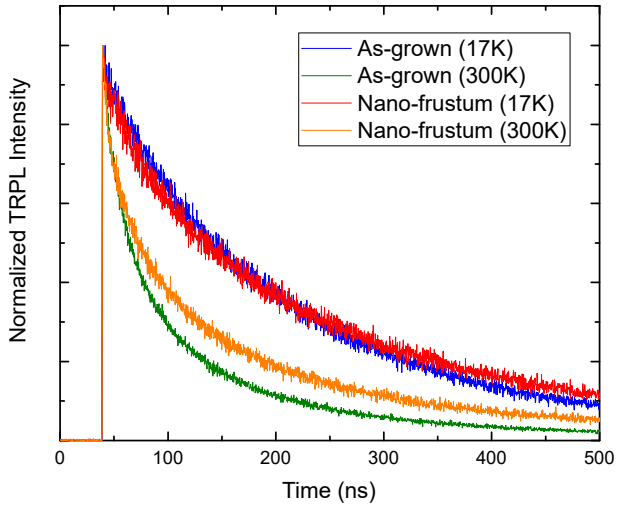

Figure 8: TRPL spectra of the strain-inducing nanostructure, corresponding to Fig. 5(b), as compared to an as-grown sample.

inverted nano-conical frustum array at 300 K and 17 K, together with the spectra from the as-grown. Using a bi-exponential decay fitting typical for multilevel system,[31] the lifetimes of the as-grown increase from 29.3 ns and 156.4 ns to 55.5 ns and 209.6 ns as the temperature decreases from 300 K to 17 K, whereas those of the nano-frustum samples rise from 37.7 ns and 216.0 ns to 49.5 ns and 258.7 ns. The increase in the room temperature TRPL decay lifetime after nanostructuring, as depicted by the longer tail as shown in Fig. 8, can be attributed to stronger QCSE due to the induced strain, consistent with findings from our previous study on the relations among strain, QCSE and PL spectral shift.[15]

The spectral red-shift with an increase in TRPL decay lifetime implies that the internal quantum efficiency (IQE) could be reduced as compared to as-grown sample without the strain-inducing nanostructures. Since an increase in Indium incorporation for a longer emission wavelength would also obviously reduce the IQE, the IQE values resulting from both red-shifting processes are determined and plotted together for comparison in Fig. 9. To estimate the IQE of the samples, low temperature PL measurements have been carried out with a setup similar to the aforementioned PL measurements, with the samples placed in a Janis cryostat. The ratio of the PL peak intensities between low temperature (12 K) and room temperature (300 K) is used to determine the IQE, as plotted in Fig. 9. Generally speaking,

the IQE at low temperature can be assumed to be 100% as the non-radiative recombination can be regarded as negligible.[32] The radiative and non-radiative lifetime can thus be calculated from the results of TRPL measurements and IQE measurements,[33,34] using the following equations[35]

$$\tau_{\mathrm{R}} = \frac{\tau_{\mathrm{TRPL}}}{\eta} \tag{1}$$

$$\tau_{\mathrm{NR}} = \frac{\tau_{\mathrm{TRPL}}}{1-\eta} \tag{2}$$

Using only the slow decay time to avoid complications, the room temperature radiative lifetime and non-radiative lifetime for the as-grown are 309.3 ns and 316.3 ns, respectively, whereas those for the nano-frustums are 530.7 ns and 364.3 ns. The increased radiative lifetime further confirms that strain induced by the nano-frustums incurs a stronger QCSE,[33,34] while the change in the non-radiative lifetime requires further investigation.

For the same epitaxial structure and emission wavelength, the IQE of the samples containing the inverted nano-conical frustum array that are etched to optimal depth are generally higher than those of the as-growns with the same emission wavelength. InGaN-based LEDs suffer from a well-known "green gap" issue[4] – the quantum efficiencies decrease as the emission wavelength increases, mainly due to issues caused by a higher Indium incorporation. Since the inverted nano-conical array has red-shifted the emission spectra without altering the Indium incorporation, the results strongly indicate that the impact on IQE using such an approach is less than growing quantum wells with higher Indium content for achieving longer emission wavelengths. The effect is increasingly prominent as the emission wavelength increase, as the IQE of the long-wavelength-emitting wafers decrease exponentially due to high Indium incorporation.[4] As the technique is purely based on top-down fabrication, it is complementary to other on-going growth-based efforts devoted at developing high-IQE long-wavelength InGaN emitters to combat the "green gap" issues. .

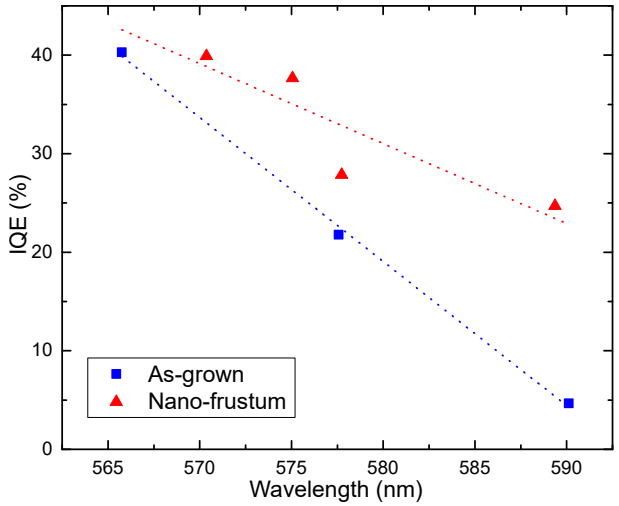

Figure 9: Comparison of the IQE between as-grown wafers and samples with strain-inducing nanostructures etched to optimal depths. Dotted lines are fitted for eye-guide purposes.

4 Conclusions

We have demonstrated an inverted nano-conical frustum array for inducing spectral red-shift by increasing strain in InGaN/GaN quantum wells for light-emitting applications. Molecular dynamics simulations show that the out-of-plane strain can be induced at the base of the nanostructure, causing a spectral red-shift of as much as ~10 nm as estimated from $\mathbf{k} \cdot \mathbf{p}$ Schrödinger calculations. Experimentally, red-shifts of up to 7.6 nm have been observed. The shortfall is explained by the existence of the tensile-strained AlGaN/GaN EBL, as well as the multiple quantum well layers at different depths that are subjected to different magnitude of strain due to the strain gradient induced by the nanostructure. The IQEs of the samples with the inverted nano-conical frustum array have been demonstrated to be higher than the as-grown counterparts at the corresponding emission wavelengths. The nanostructure design can potentially be applied for InGaN-based lighting applications with higher color rendering index (CRI) and color-tunability, as well as the monolithic integration of multiple wavelength emitters for applications such as RGB displays.

Acknowledgement

This work was supported by both General Research Funds of the Research Grant Council of Hong Kong, Project No. 17260616 and 17204218. The computations were performed using research computing facilities offered by HKU Information Technology Services.

References

(1) Penning, J.; Stober, K.; Taylor, V.; Yamada, M. Energy Savings Forecast of Solid-State Lighting in General Illumination Applications. 2016.

(2) Jang, E.; Jun, S.; Jang, H.; Lim, J.; Kim, B.; Kim, Y. White-Light-Emitting Diodes with Quantum Dot Color Converters for Display Backlights. *Advanced Materials* **2010**, *22*, 3076–3080.

(3) Anikeeva, P. O.; Halpert, J. E.; Bawendi, M. G.; Bulović, V. Quantum Dot Light-Emitting Devices with Electroluminescence Tunable over the Entire Visible Spectrum. *Nano Letters* **2009**, *9*, 2532–2536.

(4) Auf der Maur, M.; Pecchia, A.; Penazzi, G.; Rodrigues, W.; Di Carlo, A. Efficiency Drop in Green InGaN/GaN Light Emitting Diodes: The Role of Random Alloy Fluctuations. *Physical Review Letters* **2016**, *116*, 027401.

(5) Yam, F. K.; Hassan, Z. InGaN: An Overview of the Growth Kinetics, Physical Properties and Emission Mechanisms. *Superlattices and Microstructures* **2008**, *43*, 1–23.

(6) Li, K. H.; Fu, W. Y.; Choi, H. W. Chip-scale GaN integration. *Progress in Quantum Electronics* **2020**, *70*, 100247.

(7) Wu, Y. R.; Chiu, C. H.; Chang, C. Y.; Yu, P. C.; Kuo, H. C. Size-Dependent Strain Relaxation and Optical Characteristics of InGaN/GaN Nanorod LEDs. *IEEE Journal of Selected Topics in Quantum Electronics* **2009**, *15*, 1226–1233.

(8) Bocklin, C.; Veprek, R. G.; Steiger, S.; Witzigmann, B. Computational Study of an InGaN/GaN Nanocolumn Light-Emitting Diode. *Physical Review B* **2010**, *81*, 155306.

(9) Wang, Q.; Bai, J.; Gong, Y. P.; Wang, T. Influence of Strain Relaxation on the Optical Properties of InGaN/GaN Multiple Quantum Well Nanorods. *Journal of Physics D-Applied Physics* **2011**, *44*, 395102.

(10) Bai, J.; Wang, Q.; Wang, T. Characterization of InGaN-based Nanorod Light Emitting Diodes with Different Indium Compositions. *Journal of Applied Physics* **2012**, *111*, 113103.

(11) Chang, C. H.; Chen, L. Y.; Huang, L. C.; Wang, Y. T.; Lu, T. C.; Huang, J. J. Effects of Strains and Defects on the Internal Quantum Efficiency of InGaN/GaN Nanorod Light Emitting Diodes. *IEEE Journal of Quantum Electronics* **2012**, *48*, 551–556.

(12) Zhuang, Y. D.; Bruckbauer, J.; Shields, P. A.; Edwards, P. R.; Martin, R. W.; Allsopp, D. W. E. Influence of Stress on Optical Transitions in GaN Nanorods Containing a Single InGaN/GaN Quantum Disk. *Journal of Applied Physics* **2014**, *116*, 174305.

(13) Teng, C.-H.; Zhang, L.; Deng, H.; Ku, P.-C. Strain-induced Red-Green-Blue Wavelength Tuning in InGaN Quantum Wells. *Applied Physics Letters* **2016**, *108*, 071104.

(14) Feng, C.; Huang, J.-A.; Choi, H. W. Monolithic Broadband InGaN Light-Emitting Diode. *ACS Photonics* **2016**, *3*, 1294–1300.

(15) Fu, W. Y.; Choi, H. W. Explaining Relative Spectral Red-Shifts in InGaN/GaN Micropillars. *Optica* **2018**, *5*, 765–773.

(16) Plimpton, S. Fast Parallel Algorithms for Short-Range Molecular-Dynamics. *Journal of Computational Physics* **1995**, *117*, 1–19.

(17) Stillinger, F. H.; Weber, T. A. Computer-Simulation of Local Order in Condensed Phases of Silicon. *Physical Review B* **1985**, *31*, 5262–5271.

(18) Bere, A.; Serra, A. On the Atomic Structures, Mobility and Interactions of Extended Defects in GaN: Dislocations, Tilt and Twin Boundaries. *Philosophical Magazine* **2006**, *86*, 2159–2192.

(19) Zhou, X. W.; Jones, R. E. A Stillinger-Weber Potential for InGaN. *Journal of Materials Science Research* **2017**, *6*, 88–95.

(20) Zhang, L.; Yan, H.; Zhu, G.; Liu, S.; Gan, Z.; Zhang, Z. Effect of Substrate Surface on Deposition of AlGaN: A Molecular Dynamics Simulation. *Crystals* **2018**, *8*, 279.

(21) Bonfiglio, A.; Lomascolo, M.; Traetta, G.; Cingolani, R.; Di Carlo, A.; Della Sala, F.; Lugli, P.; Botchkarev, A.; Morkoc, H. Well-Width Dependence of the Ground Level Emission of GaN/AlGaN Quantum Wells. *Journal of Applied Physics* **2000**, *87*, 2289–2292.

(22) Chuang, S. L.; Chang, C. S. A Band-Structure Model of Strained Quantum-Well Wurtzite Semiconductors. *Semiconductor Science and Technology* **1997**, *12*, 252–263.

(23) Yan, Q. M.; Rinke, P.; Janotti, A.; Scheffler, M.; Van de Walle, C. G. Effects of Strain on the Band Structure of Group-III Nitrides. *Physical Review B* **2014**, *90*, 125118.

(24) Fu, W. Y.; Wong, K. K.-Y.; Choi, H. W. Close-Packed Hemiellipsoid Arrays: A Photonic Band Gap Structure Patterned by Nanosphere Lithography. *Applied Physics Letters* **2009**, *95*, 133125.

(25) Fu, W. Y.; Wong, K. K.-Y.; Choi, H. W. Room Temperature Photonic Crystal Band-Edge Lasing from Nanopillar Array on GaN Patterned by Nanosphere Lithography. *Journal of Applied Physics* **2010**, *107*, 63104.

(26) Li, K. H.; Choi, H. W. Air-Spaced GaN Nanopillar Photonic Band Gap Structures Patterned by Nanosphere Lithography. *Journal of Applied Physics* **2011**, *109*, 023107.

(27) Zhang, Q.; Li, K. H.; Choi, H. W. InGaN light-Emitting Diodes with Indium-Tin-Oxide Sub-Micron Lenses Patterned by Nanosphere Lithography. *Applied Physics Letters* **2012**, *100*, 061120.

(28) Ogiya, H.; Nishimiya, T.; Hiramoto, M.; Motoyama, S.; Tsuji, O. Chlorine-Based ICP Etching for Improving the Luminance Efficiency in Nitride LEDs. Proceedings of the 2012 International Conference on Compound Semiconductor Manufacturing.

(29) Lu, J.-Y.; Deng, D.-M.; Wang, Y.; Chen, K. J.; Lau, K.-M.; Zhang, T.-Y. Phonon Deformation Potentials of Hexagonal GaN Studied by Biaxial Stress Modulation. *AIP Advances* **2011**, *1*, 032132.

(30) Demangeot, F.; Frandon, J.; Renucci, M. A.; Briot, O.; Gil, B.; Aulombard, R. L. Raman Determination of Phonon Deformation Potentials in α-GaN. *Solid State Communications* **1996**, *100*, 207–210.

(31) Özgür, U.; Fu, Y.; Moon, Y. T.; Yun, F.; Morkoç, H.; Everitt, H. O.; Park, S. S.; Lee, K. Y. Long Carrier Lifetimes in GaN Epitaxial Layers Grown Using TiN Porous Network Templates. *Applied Physics Letters* **2005**, *86*, 232106.

(32) Titkov, I. E.; Karpov, S. Y.; Yadav, A.; Zerova, V. L.; Zulonas, M.; Galler, B.; Strassburg, M.; Pietzonka, I.; Lugauer, H.; Rafailov, E. U. Temperature-Dependent Internal Quantum Efficiency of Blue High-Brightness Light-Emitting Diodes. *IEEE Journal of Quantum Electronics* **2014**, *50*, 911–920.

(33) Ajia, I. A.; Yamashita, Y.; Lorenz, K.; Muhammed, M. M.; Spasevski, L.; Almalawi, D.; Xu, J.; Iizuka, K.; Morishima, Y.; Anjum, D. H.; Wei, N.; Martin, R. W.; Kuramata, A.; Roqan, I. S. GaN/AlGaN Multiple Quantum Wells Grown on Transparent and Conductive (-201)-Oriented β-Ga_2O_3 Substrate for UV Vertical Light Emitting Devices. *Applied Physics Letters* **2018**, *113*, 082102.

(34) Sun, H.; Mitra, S.; Subedi, R. C.; Zhang, Y.; Guo, W.; Ye, J.; Shakfa, M. K.; Ng, T. K.; Ooi, B. S.; Roqan, I. S.; Zhang, Z.; Dai, J.; Chen, C.; Long, S. Unambiguously Enhanced Ultraviolet Luminescence of AlGaN Wavy Quantum Well Structures Grown on Large Misoriented Sapphire Substrate. *Advanced Functional Materials* **2019**, *29*, 1905445.

(35) Minsky, M. S.; Watanabe, S.; Yamada, N. Radiative and Nonradiative Lifetimes in GaInN/GaN Multiquantum Wells. *Journal of Applied Physics* **2002**, *91*, 5176–5181.

Graphical TOC Entry